Reversible Optical Storage Properties of Nanostructured Epoxy-Based Thermosets Modified with Azobenzene Units

Raquel Fernández, Jose Angel Ramos, Leandro Espósito,

Agnieszka Tercjak, Iñaki Mondragon*

‘Materials + Technologies’ Group, Department of Chemical & Environmental Engineering, Polytechnic School, Universidad del País Vasco/Euskal Herriko Unibertsitatea, Pza Europa 1, 20018 Donostia-San Sebastián, Spain

* Corresponding author. Tel.: +34 943 017 177; fax: +34 943 017 130.

E-mail address: inaki.mondragon@ehu.es (I. Mondragon)

ABSTRACT

Azo-containing polymers are of particular interest in the design of materials for applications in optical recording. The aim of this contribution was the synthesis and characterisation of optically active epoxy-based nanostructured thermosets obtained using epoxidized poly(styrene-*b*-butadiene-*b*-styrene) (SBS) as templating agent and modified with azobenzene groups. Morphological analysis by means of atomic force microscopy, as well as an investigation about the anisotropic optical properties of the developed materials was carried out. Different types of morphologies from micelles without long-range order to nanostructures with long-range order were achieved depending on the content of epoxidized block copolymer and azobenzene, and on the extent of epoxidation of butadiene blocks. In addition, the study of optical anisotropy showed a clear dependence of the optical storage properties upon the concentration of azo-chromophore in the samples. In particular, a thermoset containing 12.3 wt% of azo-dye and 5 wt% of SBS with 46 mol% of butadiene blocks epoxidized revealed a spherical micellar morphology with maximum birefringence in the order of $1.8 \cdot 10^{-2}$ and residual fraction of birefringence of around 0.3 after several weeks of turning *off* the writing beam. Besides, numerous writing-erasing cycles could also be performed without photo-degradation of the materials. Furthermore, comparing parent thermosets and nanostructured systems, similar birefringence values were obtained with the advantage that the latter can also be used as templates for the development of multifunctional advanced thermosetting materials with optical properties.

Keywords: epoxy; azobenzene; block-copolymer; nanostructuring; birefringence

INTRODUCTION

Over the last years, photonics has emerged as a major interdisciplinary field of science and technology with a focus on the transport and manipulation of light. Rapid progress in photonics has been achieved because of continuous advances in nanotechnology, materials science, optics, physics, among other areas.[1]

Polymers play an important role in the development of materials for photonics. They are relatively inexpensive materials that can be functionalized to achieve required properties, they themselves can possess useful optical properties like photoluminescence, and they can also act as matrices for optically active species such as inorganic nanoparticles, quantum dots, liquid crystals or dyes.[1-6] Notably, azobenzene serves as the parent molecule to a wide range of dyes and non-linear optical chromophores. In addition, changes that can be imparted to polymers when azobenzene is part of their structures or is associated with them can help to develop new applications in the field. Indeed, reversible photo-isomerisation in azo-containing polymers enables the use of light as a powerful external stimulus to control or trigger the change of the properties of these materials. For this reason, there has been considerable worldwide research devoted to azo-polymers, ranging from fundamental studies to exploitation for applications. Most research has dealt with the physical and optical properties of azo-polymers interesting for applications in the area of reversible optical storage.[7-13]

Epoxy resins represent a family of thermosetting polymers known from many decades ago. The wide diffusion they have found on the market is a consequence of their extreme versatility and their excellent attributes, such as abrasion resistance, thermal

stability, chemical resistance and mechanical properties. Those features make them primary candidates for a wide range of applications among which epoxy thermosets stand out as high performance matrices in advanced composites, coatings, adhesives and laminates. Thus, researchers have focused mainly on the study of their mechanical and thermal properties.[14-16] However, epoxy networks are also transparent and, therefore, suitable for optical applications, even though these have not been explored so much as the mechanical ones.

On this basis and taking into account the need for new materials with specific functionalities appropriate for emerging technological applications, preparation of thermosets based on epoxy resins for optical applications can be of interest. In addition, nanostructured thermosets are a relatively new class of advanced materials which are able to improve the mechanical properties of conventional thermosetting polymers retaining their optical transparency.[17-19] In fact, block copolymers (BCP), owing to their capability to form nanoscale structures, are widely used as templates for generating nanostructured epoxy matrices with long-range order.[20-23] One way to achieve this goal is through reaction-induced microphase separation (RIMS) of one of the blocks during curing, both being initially miscible with the epoxy resin. In the case of BCP with both blocks immiscible with the epoxy system after curing, one feasible approach to promote the compatibilisation of one of the blocks with the epoxy matrix can be its chemical modification. For instance, poly(styrene-*b*-butadiene-*b*-styrene) (SBS) block copolymers can be randomly-epoxidized with this objective. This methodology has been satisfactorily employed in our group to generate stable nanostructures in epoxy matrices.[24, 25] Additionally, nanostructured thermosetting systems can also act as a template for the incorporation of inorganic nanoparticles with particular properties with

the aim of developing multifunctional materials, which is the current challenge of many researchers.[26]

The present work is oriented towards the development of novel nanostructured epoxy systems containing azobenzene groups for reversible optical storage. With this goal in mind, azo-containing epoxy/amine formulations were modified with epoxidized SBS to promote the compatibilisation of the polybutadiene (PB) block with the epoxy matrix. On this way nanostructured epoxy thermosets containing azobenzene groups have been achieved, due to reaction-induced microphase separation of polystyrene (PS) block. Optical and morphological properties of the resulting nanostructured materials were evaluated and discussed considering several variables as epoxidation extent, epoxidized SBS content and azobenzene concentration in the epoxy matrix.

EXPERIMENTAL

Synthesis of azo-containing nanostructured epoxy thermosets

Materials

Amphiphilic linear SBS block copolymer, C540, with 40 wt% PS was kindly supplied by Repsol-YPF. A push-pull azo-dye, 4-(4-nitrophenylazo)aniline $(O_2N)(C_6H_4)N=N(C_6H_4)(NH_2)$, Disperse Orange 3 (DO3), with a melting temperature of 200 ºC, was purchased from Aldrich. An epoxy resin, diglycidyl ether of bisphenol A (DGEBA), DER 332 n = 0.03, with an epoxy equivalent of 175 g eq^{-1}, was kindly provided by Dow Chemical. As hardener we employed an aromatic diamine, 4,4'-methylene-bis(3-chloro-2,6-diethylaniline) (MCDEA), supplied by Lonza. All materials were used as received without further purification.

Different randomly-epoxidized SBS block copolymers, $SBSep_x$ (x being the extent of epoxidation, mol%, with respect to PB double bonds determined by ^1H NMR), were obtained by epoxidation of PB blocks. This reaction was carried out using hydrogen peroxide in the presence of an *in situ* prepared catalyst system in a water/dichloroethane biphasic mixture, following a procedure described elsewhere.[24]

Curing protocol

A thermoplastic azo-prepolymer (TAZ) was synthesized by reaction between DO3 and DGEBA following a procedure previously described.[27] It was prepared in a stoichiometric ratio r = DO3 eq/DGEBA eq = 0.5 to achieve reaction products with epoxy groups in the extreme of chains. Then, TAZ was blended in different ratios (10, 20 or 50 wt%) with DGEBA, MCDEA and various amounts of $SBSep_x$ (from 5 to 50 phr) to prepare different azo-containing epoxy systems. Dichloroethane was used as solvent to obtain homogeneous samples. Before curing the solvent was removed by evaporation at room temperature. All samples were then cured at 140 ºC during 24 h and post-cured at 165 ºC for 2 h. An amino-hydrogen-to-epoxy stoichiometric ratio equal to 1 was maintained for all prepared systems. A brief description of all samples studied is presented in Table 1. Epoxy thermosets without BCP were named according to their content in thermoplastic azo-prepolymer as TAZy (y being TAZ ratio (wt%)). Nanostructured systems were named according to their content both in TAZ and epoxidized SBS as TAZy-$SBSep_x$z (z being $SBSep_x$ ratio (phr)).

Characterisation of azo-containing nanostructured epoxy thermosets

Differential scanning calorimetry measurements

Differential scanning calorimetry (DSC) was performed using a Mettler Toledo DSC

192 822 differential scanning calorimeter equipped with a sample robot 193 TSO 801 RO. Nitrogen was used as purge gas (10 mL min^{-1}). The glass transition temperature (T_g), defined as the onset of the change in specific heat, was determined from the thermograms obtained in heating scans at 10 ºC min^{-1}.

Morphological analysis

For the morphological study the reactive solutions were drop cast into polytetrafluoroethylene moulds of 4 cm x 4 cm x 1 cm. After that, the solvent was removed and the curing schedule described above was performed. Samples of cured mixtures were prepared using an ultramicrotome (Leica Ultracut R) equipped with a diamond knife.

The morphology of the samples was studied by atomic force microscopy (AFM). AFM images were obtained with a Nanoscope IIIa scanning probe microscope (Multimode™, Digital Instruments). Tapping mode (TM) in air was employed using an integrated tip/cantilever (125 μm in length with *ca* 300 kHz resonant frequency and spring constant of *ca* 40 N/m). Typical scan rates during recording were 0.7-1 line s^{-1} using a scan head with a maximum range of 16 μm x 16 μm.

Optical analysis

For the analysis of optical properties films of all nanostructured systems were prepared onto clean glass slides by spin-coating from 5 wt% reactive solutions in dichloroethane, using a P6700 spin-coater from Cookson Electronics. The spinner program was 1000 rpm for 30 s and 2000 rpm for 30 s or 200 rpm for 60 s and 1000 rpm for 30 s, depending on the required thickness. Residual solvent was removed by evaporation at

room temperature and, then, samples were cured following the experimental conditions mentioned above. Film thicknesses were calculated from topographic AFM images of scratched films, taking into account the difference in height between a flat area of the sample and the surface of the clean glass slide. Relatively homogeneous thin films of variable thicknesses between 500 ± 50 nm and 1000 ± 100 nm were obtained.

Optical storage experiments were carried out at room temperature and under ambient conditions. The experimental setup used was similar to that previously reported.[27] Optical birefringence was induced in films of the obtained azo-containing materials using a linearly polarised argon laser operating at 488 nm (writing beam) with a polarisation angle of 45º with respect to the polarisation direction of a low power He-Ne laser operating at 632.8 nm (reading beam). The power of the writing beam used in the experiments was varied between 4 and 24 mW on a spot of 0.4 mm^2 and the change in the transmission of the reading beam, which passed through the sample between two crossed polarisers, was measured with a photodiode. The induced birefringence (Δn) was determined by measuring the reading beam transmission ($T = I/I_0$) according to:

$$\Delta n = (\lambda/\pi\, d)\, \sin^{-1}\, (I/I_0)^{1/2}$$

where λ is the wavelength of the reading beam, d is the film thickness, I is the intensity of the reading beam after the second polariser and I_0 is the transmitted intensity of the reading beam between parallel polarisers in absence of anisotropy.

Previous to optical experiments films were heated above T_g of the epoxy thermosets and subsequently stored at room temperature. In addition, each photo-orientation experiment

was done on a different previously non-irradiated spot so as to avoid irradiation history complications.

RESULTS AND DISCUSSION

Morphological analysis

Nanostructured epoxy systems containing an azo-dye were achieved by modification with epoxidized SBS block copolymer. Specifically, azobenzene groups were introduced via chemical bonding between TAZ and DGEBA/MCDEA system, the thermoplastic azo-prepolymer being therefore part of the epoxy matrix. All the epoxy-based networks studied had the azo-chromophore placed in a branch, also called crosslinked side chain.[12]

The morphologies generated were investigated using TM-AFM. In particular, the effects of azobenzene content, epoxidized SBS ratio and epoxidation extent of butadiene blocks on nanostructuring were analysed. As shown in our previous work,[28] random epoxidation of PB block at high extent leads to miscibility of this block with the epoxy matrix and segregation of PS block during network formation, thus achieving long-range order nanostructures. It should be noted that in this work TAZ was part of the epoxy network, which withdrew PS chains during curing. As published by Ocando et al.,[25] it has to be taken into account that two different mechanisms can be involved through morphology development during curing as a function of epoxidized PB content in DGEBA/MCDEA systems modified with epoxidized SB block copolymers. On the one hand, reaction-induced microphase separation of PS block leads to long-range order nanostructures and, on the other hand, combination of both self-assembly of epoxidized PB block in the initial mixture and RIMS of PS block can give rise to vesicles or long

worm-like micelles with a bilayered structure.[25] In this work, additionally, we found that the presence of the thermoplastic azo-prepolymer provoked a decrease of miscibility of initial mixtures before curing, leading to different morphologies as a function of TAZ content owing to the modification of interactions between groups with respect to the modified matrices without TAZ, as discussed below.

Figure 1 shows TM-AFM phase images of cured epoxy systems modified with different amounts of $SBSep_{37}$ (10 and 30 phr) containing several TAZ ratios (10, 20 and 50 wt%). This epoxidation extent (37 mol%) was above the miscibility threshold with the epoxy resin.[28] Only phase images are shown due to the resemblance of height and phase TM-AFM images of each sample. As can be observed, in all cases microphase separation was achieved. TAZ10-$SBSep_{37}$10 cured epoxy system showed micellar nanodomains of PS block in the epoxy matrix. The size of these microphase-separated domains was around 30 nm in diameter. Increasing of the thermoplastic azo-prepolymer content to 20 wt% (TAZ20-$SBSep_{37}$10) led to higher amount of segregated domains. For TAZ50-$SBSep_{37}$10 cured system coexistence of nanodomains with around 30 nm in diameter, interconnected long worm-like micelles and spherical structures was achieved. These morphological variations were probably related to the fact that increasing TAZ content, the miscibility between the block copolymer and the epoxy system before curing decreased. Here it should be pointed out that PS homopolymer is miscible with DGEBA/MCDEA system at temperatures higher than 90 ºC.[25] On the other side, increasing of the PB epoxidation extent and the ratio between pure epoxy resin and TAZ led to higher compatibility between the block copolymer and the epoxy matrix. Therefore, taking into account the initial miscibility of blocks with the epoxy system before curing, for 37 mol% of epoxidation extent one can expect the formation

of segregated structures in the epoxy matrix through self-assembly of epoxidized PB occurred prior to curing, followed by fixing these structures through reaction-induced microphase separation of PS chains during network formation. Results confirmed that for investigated systems this process was favoured by the increase of TAZ content. Thus, various morphologies, through combination of self-assembly of PB block and RIMS of PS block, were generated as consequence of variations in interactions between groups in the initial mixtures.

In addition, increase of PS content with increasing $SBSep_{37}$ content from 10 to 30 phr led to longer segregated structures. As reported by Ocando et al.,[28] for enough PB epoxidation, the morphologies generated in the same kind of thermosetting systems without azo-dye depend strongly on PS content in the initial mixture. On the other side, it is worth to note that larger segregated structures were achieved for thermosetting systems with 30 phr $SBSep_{37}$ as increasing TAZ content, due to a decrease of miscibility between the epoxy-precursor mixture and the block copolymer that led to self-assembled segregation of some amount of PB block before curing.

Furthermore, as shown in Figures 2-4, increase of the epoxidation extent provoked higher miscibility between epoxidized PB block and epoxy matrix and, consequently, long-range order nanostructures were achieved. Indeed, when increasing the epoxidation extent from 37 up to 46 mol% (Figure 2), the system containing 10 wt% TAZ and 50 phr BCP revealed PS cylinders inside the matrix mixture. The thermosetting system containing 20 wt% TAZ and 20 phr BCP showed worm-like structures (Figure 3), while for the system containing 50 wt% TAZ and 5 phr BCP spherical micellar nanostructures were achieved (Figure 4) with the same increase in the

epoxidation extent.

According to previous work done in our group,[25] as well as by other authors, such as Dean et al.[21] who established that for low contents of block copolymer phase transitions from spherical micelles to worm-like micelles and, finally, to vesicles took place as the volume fraction of immiscible block increased, results presented here suggest that 46 mol% of epoxidation extent was needed to achieve long-range order nanostructuring because of the higher compatibility of the more epoxidized SBS with the epoxy-precursor mixture. Consequently, for 46 mol% of epoxidation extent morphologies were originated through reaction-induced microphase separation of PS block starting from a miscible mixture before curing. On the contrary, 37 mol% of epoxidation extent was not enough to make compatible all not randomly-epoxidized PB chains with the epoxy-precursor mixture before curing. Thus, morphologies were developed through self-assembly before curing followed by fixing the nanostructures via phase separation of PS chains through curing reaction, leading to different segregated structures depending on the content of block copolymer and thermoplastic azo-prepolymer. Furthermore, miscibilisation of initial mixtures was favoured not only as increasing the epoxidation extent, but also as decreasing TAZ content, since a significant amount of randomly-epoxidized PB chains could not be miscibilised before curing when high quantities of TAZ were incorporated into the epoxy system.

Analysing together Figures 1-4 and focusing on $SBSep_{37}$ content, for the lowest azobenzene ratio (10 wt% TAZ) the morphology evolved from micelles with around 30 nm in diameter for 10 phr $SBSep_{37}$ (Figure 1a) to worm-like nanostructures without long-range order for 50 phr $SBSep_{37}$ (Figure 2a). For the sample with 20 wt% TAZ

longer microphase-separated structures were achieved when increasing $SBSep_{37}$ content from 10 to 30 phr (Figures 1b-3a-1e). Finally, for the highest azobenzene content (50 wt% TAZ), various morphologies were achieved as a function of $SBSep_{37}$ ratio. TAZ50-$SBSep_{37}$5 cured epoxy system (Figures 4a) showed a combination of separated nanodomains with around 30 nm in diameter and spherical structures. For TAZ50-$SBSep_{37}$10 (Figures 1c) in addition interconnected long worm-like micelles appeared and for TAZ50-$SBSep_{37}$30 (Figures 1f), as the ratio of segregated block copolymer increased, the morphology evolved to a geometry with less interfacial curvature.

Optical analysis

In relation to the optical storage abilities of azo-containing materials, the information is stored in the form of photo-induced anisotropy in this kind of systems.[29] Optical anisotropy is a birefringence optically induced in polymeric films as a result of a reorientation of the azo-chromophores via a statistical selection process. Normally, linearly polarised light is employed to provoke a *trans-cis* isomerisation followed by a molecular reorientation and a *cis-trans* isomerisation. The absorption and reorientation sequence will be repeated until the azobenzene molecules dipole moment lies in a direction which is perpendicular to the polarisation direction of the writing beam. Working on the principle that some of the fundamental attributes a material requires to be employed as an optical memory media are high storage capacity, fast response, stability during writing-erasing cycles and long-term stability. The parameters we wanted to investigate were the maximum level of achievable birefringence and the rate of birefringence growth, as well as the thermal relaxation rate and the long-term stability of the induced birefringence. In addition, there are a series of aspects affecting those variables, including chemical factors (such as type of azo-chromophore,

azobenzene content, T_g, structure of the polymeric main chain, …) and physical ones (such as irradiation wavelength and intensity, film thickness, history of the sample, operating temperature …).[10, 13, 30-34] All of them were taken into consideration in the present work.

Firstly, the maximum anisotropy that can be photo-induced in the samples was evaluated. Table 2 shows the birefringence values and glass transition temperatures of all prepared epoxy systems. Since birefringence depends on the azobenzene quantity, Δn_N values, the birefringence data normalised to the azo-dye content (Δn divided by wt% DO3), have also been reported. As can be seen, Δn data varied from $0.2 \cdot 10^{-2}$ to $1.9 \cdot 10^{-2}$ as the azo-chromophore increased from 1.72 to 12.9 wt%. These birefringence values can be considered adequate for optical applications taking into account the low azobenzene concentrations used and the reported values for this kind of materials.[35-37] Nevertheless, it should be noted that no significant differences in Δn_N could be seen between parent azo-containing thermosets and the ones modified with epoxidized SBS. Therefore, nanostructuring did not have a significant influence on the maximum level of achievable birefringence, which means the interactions among azobenzene groups were similar in both kind of systems, because in all cases they were covalently linked to the epoxy network via chemical bonding between TAZ and DGEBA/MCDEA system. However, a slight increase in Δn_N was perceptible when increasing TAZ content, probably due to an increase of interactions between azobenzene units, as a consequence of the increase in azo-dye concentration.

The formation, relaxation and erasing of birefringence is illustrated in a more descriptive way in Figure 5 by writing-relaxing-erasing sequences obtained for the

systems TAZ10, TAZ20 and TAZ50 with 30 wt% $SBSep_{37}$. Initially there was no transmission of the reading beam, which continuously illuminated the samples, since azobenzene molecules in *trans* form were randomly distributed. At point *A*, the writing beam was turned *on* and the reading beam was transmitted through the crossed polarisers due to the optical anisotropy induced in the films as a consequence of *trans-cis-trans* photo-isomerisations that led to the orientation of *trans* molecules perpendicular to the polarisation vector of the writing beam. In consequence, birefringence was rapidly built up to the saturation level. Indeed, the optical anisotropy level increased as the azobenzene content was higher, since Δn is the result of photo-induced orientation of the azo-chromophores. Hence, larger number of photo-active units in the polymer chains generated a higher birefringence. This photo-induced anisotropy represents a writing mechanism in an optical storage device. When the writing beam was turned *off* at point *B*, Δn rapidly fell *off* initially, due to thermally activated dipole reorientation which would tend towards randomisation of the anisotropy. Thereafter, Δn became stable in a relaxed level, where the rate of change of anisotropy was very small. This fact proved that the birefringence was not completely preserved after writing with linear polarised light, even though a significant amount of optically induced orientation was conserved. The stable birefringence pattern or remaining birefringence corresponds to the storage step. Finally, at point *C*, in order to remove the remaining birefringence, circularly polarized light was introduced, which completely eliminated the dipole orientation. This mode of writing effectively returned the films to the isotropic state, thereby erasing the previously encoded information.

Focusing on the rate of birefringence growth, the time interval necessary to achieve 80% of saturated birefringence level, t^{80}, is plotted in Figure 6. In particular, Figure 6a

shows the influence of azobenzene concentration, $SBSep_{37}$ content and film thickness in the time necessary to photo-induced anisotropy when films were irradiated with 6 mW of beam power. As it is shown, t^{80} was clearly reduced when increasing the azobenzene content in the samples. This behaviour can be explained in terms of a thermal effect. That is to say, an increase in the writing beam absorption occurred upon increasing the azo-chromophore concentration, which could induce sample heating.[38] This heating allowed a higher molecular mobility and resulted in a faster writing process. Moreover, t^{80} increased when increasing the amount of $SBSep_{37}$ in the samples. The increase in $SBSep_{37}$ content implied a decrease of global DO3 ratio and T_g value. The glass transition temperature can be useful as an approach to predict the freedom of movement of azobenzene units in the epoxy network. The lower the T_g value, the higher the molecular mobility. Based on this assumption, t^{80} should decrease as increasing $SBSep_{37}$ content. But the dependence of azobenzene concentration has also to be considered. By increasing the azo-dye content in the samples, t^{80} decreased even though T_g values were higher. Thus, one can conclude that the thermal effect due to the optical absorption of azobenzene moieties in the wavelength region of the recording light had higher influence on the rate of birefringence growth than the glass transition temperature over the range of values studied. Additionally, in order to analyse the effect of film thickness on the writing rate, t^{80} of films with 50 wt% TAZ and the same $SBSep_{37}$ content (0 and 10 wt%) but different thickness (500 ± 30 nm or 1000 ± 10 nm) were compared. A slow down of the writing rate was noticed upon increasing the samples thickness. This result may be connected to the fact that as the film thickness increased, the intensity of the writing beam considerably decreased as it propagated throughout the sample, due to large laser intensity absorption of the azobenzene moieties. As a result, the rate of birefringence growth decreased, which is in good

agreement with the work reported by Rochon et al.[30] devoted to the study of film thickness effect on net phase retardation and writing speed in azo-polymers.

Concerning the influence of the writing intensity on t^{80}, as depicted in Figure 6b, the writing rate grew with the increase in laser beam power. As reported by Natansohn et al.,[39] the writing times are controlled by the photon flux, confirming the statistical nature of the process. That is to say, the writing rate was dependent on the number of photons involved in the writing process. The more photons the sample absorbed, the more possible azo-chromophores orientations and the lower t^{80}.

In general, relaxation processes are easier to be studied than orientation ones since effects of heating and isomerisation rates are small when the writing beam is turned *off*. Parameters that have a clear influence on the remaining birefringence are glass transition temperature and cooperative effects that may cause relaxation times to be longer with the increase in azo-chromophore content.[29] Figure 7a shows the percentage of remaining birefringence after 60 s of turning *off* the writing beam (rem^{60}) at 6 mW as a function of $SBSep_{37}$ ratio and azobenzene concentration in the epoxy thermosets, regardless of films thickness. At higher azo-chromophore contents, the epoxy systems exhibited higher rem^{60}. Furthermore, as can be seen in Table 3, the remaining birefringence increased with the azobenzene concentration in samples with similar T_g values, suggesting that, for the systems studied, the main factor affecting rem^{60} was the azo-dye content. However, a *plateau* for DO3 contents above 4 wt% was reached, which could indicate that, for these epoxy thermosets and in the range of values evaluated, rem^{60} depended mainly on cooperative interactions among azobenzene groups up to an azo-dye concentration from which the remaining birefringence kept

constant.

Nevertheless, it should be pointed out that T_g values of the thermosets prepared varied from 79 to 155 ºC, which should favour a good orientation stability of the photo-active chromophores at room and slightly elevated temperatures. Hence, we also studied the long-term stability of the induced birefringence. The residual fraction of birefringence after 45 h of turning *off* the writing beam at 6 mW for a film of TAZ50-SBSep$_{46}$5 is plotted in Figure 7b. During the first 4 min of turning *off* the writing beam, birefringence was relaxed around 30%. Then, after 10 h the residual fraction of birefringence was about 0.3 and, though not shown here, it kept stable during several weeks.

Our ultimate interest was to study the rewriting stability of the samples. In particular, it was analysed the maximum transmitted intensity of the reading beam after passing through a film of TAZ20-SBSep$_{37}$10 during 270 writing-erasing cycles (Figure 8). During the first 10 cycles up to around 30 cycles, similar transmitted signal was achieved. After 60 writing-erasing sequences in the order of 60% of maximum intensity was still registered and after 140 cycles 50% of maximum intensity was achieved. Finally, after 270 cycles almost 40% of maximum transmitted signal was reached, which means that after 270 cycles there was still a significant birefringence that could be used to distinguish the *on* from the *off* state. Therefore, the ability of this nanostructured epoxy-based thermoset containing azobenzene groups for rewriting was found adequate after consecutive cycles.

CONCLUSIONS

Nanostructured thermosets with different morphologies were obtained from epoxy systems containing azobenzene units using epoxidized SBS as templating agent.

Concerning the morphological study by AFM the main conclusion that can be drawn from this work is that depending on the epoxidation extent and the content of epoxidized SBS and TAZ, nanostructuring of investigated thermosetting systems took place in different ways. For the lowest epoxidation extent (37 mol%), the formation of nanostructures followed the combined mechanisms of self-assembly of PB chains and reaction-induced microphase separation of PS chains through curing. In addition, self-assembly mechanism was favoured when increasing TAZ content in the samples, due to a decrease of miscibility between the epoxy-precursor mixture and the block copolymer before curing. Upon increasing the epoxidation extent to 46 mol%, long-range order nanostructures through RIMS of PS block were achieved for the samples with 10 and 20 wt% TAZ containing 50 and 20 phr BCP, respectively, owing to a higher compatibility of the block copolymer with the epoxy-precursor mixture.

With respect to the analysis of reversible optical storage properties in the developed materials, over the range of values evaluated for the used chromophore and polymer matrix, the azo-dye content was the main factor influencing the optical properties. For very low azobenzene contents (<4 wt%), the poor interaction among photo-active units led to a decrease of Δn_N and remaining birefringence values. However, from around 4 wt% of azo-dye the remaining birefringence and Δn_N kept almost constant in both parent thermosets and the ones modified with epoxidized SBS. Hence, nanostructuring did not have a significant effect on birefringence, because in all studied systems the azo-

chromophores were covalently linked to the epoxy-rich phase, and therefore interactions among azobenzene moieties were similar in parent and nanostructured thermosets. Nonetheless, these systems nanostructured by BCP addition could also be used as templates to develop multifunctional materials, for instance by selective dispersion of nanoparticles, thus giving rise to advanced hybrid nanostructured thermosets with interesting combined properties.

ACKNOWLEDGEMENTS

Financial support from the EU (Carbon nanotube confinement strategies to develop novel polymer matrix composites, POCO, FP7-NMP-2007, CP-IP 213939-1), Basque Country Government in the frame of Grupos Consolidados (IT-365-07), inanoGUNE (IE09-243), NANOTES (S-PE10UN40) and from the Spanish Ministry of Education and Science (MAT2009-12832) is gratefully acknowledged. The authors also thank the technical and human support provided by SGIker (Macrobehaviour-Mesostructure-Nanotechnology unit). R. Fernández acknowledges the University of the Basque Country for the grant 'Ayuda para la Especialización de Doctores en la UPV/EHU'.

REFERENCES

(1) Paquet, C.; Kumacheva, E. *Mater. Today* **2008**, *11*, 48-56.

(2) Jiang, H.-J.; Gao, Z.-Q.; Liu, F.; Ling, Q.-D.; Wei, W.; Huang, W. *Polymer* **2008**, *49*, 4369-4377.

(3) Hanemann, T.; Szabó, D. V. *Materials* **2010**, *3*, 3468-3517.

(4) Hu, L.; Wu, H.; Du, L.; Ge, H.; Chen, X.; Dai, N. *Nanotechnology* **2011**, *22*, 125202 (6pp).

(5) Dierking, I. *Polym. Chem.* **2010**, *1*, 1153-1159.

(6) Pucci, A.; Bizzarri, R.; Ruggeri, G. *Soft Matter* **2011**, *7*, 3689-3700.

(7) Kumar, G. S.; Neckers, D. C. *Chem. Rev.* **1989**, *89*, 1915-1925.

(8) Viswanathan, N. K.; Kim, D. Y.; Bian, S.; Williams, J.; Liu, W.; Li, L.; Samuelson, L.; Kumar, J.; Tripathy, S. K. *J. Mater. Chem.* **1999**, *9*, 1941-1955.

(9) Delaire, J. A.; Nakatani, K. *Chem. Rev.* **2000**, *100*, 1817-1846.

(10) Natansohn, A.; Rochon, P. *Chem. Rev.* **2002**, *102*, 4139-4175.

(11) Yesodha, S. K.; Sadashiva Pillai, C. K.; Tsutsumi, N. *Prog. Polym. Sci.* **2004**, *29*, 45-74.

(12) Oliveira Jr, O. N.; Dos Santos Jr, D. S.; Balogh, D. T; Zucolotto, V.; Mendonça, C. R. *Adv. Colloid Interface Sci.* **2005**, *116*, 179-192.

(13) Zhao, Y.; Ikeda, T. *Smart light-responsive materials: azobenzene-containing polymers and liquid crystals*; Hoboken, New Jersey: John Wiley & Sons, 2009.

(14) Fdez. de Nograro, F.; Llano-Ponte, R.; Mondragon, I. *Polymer* **1996**, *37*, 1589-1600.

(15) Ramos, J. A.; Blanco, M.; Zalakain, I.; Mondragon, I. *J. Colloid Interface Sci.* **2009**, *336*, 431-437.

(16) Leonardi, A. B.; Fasce, L. A.; Zucchi, I. A.; Hoppe, C. E.; Soulé, E. R.; Pérez, C. J.; Williams, R. J.J. *Eur. Polym. J.* **2011**, *47*, 362-369.

(17) Kosonen, H.; Ruokolainen, J.; Nyholm, P.; Ikkala, O. *Polymer* **2001**, *42*, 9481-9486.

(18) Leibler, L. *Prog. Polym. Sci.* **2005**, *30*, 898-914.

(19) Jaffrennou, B.; Portal, J.; Méchin, F.; Pascault, J. P. *Eur. Polym. J.* **2008**, *44*, 3439-3455.

(20) Ritzenthaler, S.; Court, F.; David, L.; Girard-Reydet, E.; Leibler, L.; Pascault, J. P. *Macromolecules* **2002**, *35*, 6245-6254.

(21) Dean, J. M.; Grubbs, R. B.; Saad, W.; Cook, R. F.; Bates, F. S. *J. Polym. Sci.: Part B: Polym. Phys.* **2003**, *41*, 2444-2456.

(22) Hermel-Davidock, T. J.; Tang, H. S.; Murray, D. J.; Hahn, S. F. *J. Polym. Sci., Part B: Polym. Phys.* **2007**, *45*, 3338-3348.

(23) Fan, W.; Wang, L.; Zheng, S. *Macromolecules* **2010**, *43*, 10600-10611.

(24) Serrano, E.; Larrañaga, M.; Remiro, P.M.; Mondragon, I.; Carrasco, P. M.; Pomposo, J. A.; Mecerreyes, D. *Macromol. Chem. Phys.* **2004**, *205*, 987-996.

(25) Ocando, C.; Tercjak, A.; Martín, M. D.; Ramos, J. A.; Campo, M.; Mondragon, I. *Macromolecules* **2009**, *42*, 6215-6224.

(26) Gutierrez, J.; Tercjak, A.; Mondragon, I. *J. Phys. Chem. C* **2010**, *114*, 22424-22430.

(27) Fernández, R.; Mondragon, I.; Oyanguren, P. A.; Galante, M. J. *React. Funct. Polym.* **2008**, *68*, 70-76.

(28) Ocando, C.; Tercjak, A.; Serrano, E.; Ramos, J. A.; Corona-Galván, S.; Parellada, M. D.; Fernández-Berridi, M. J.; Mondragon, I. *Polym. Int.* **2008**, *57*, 1333-1342.

(29) Mendoça, C. R.; dos Santos Jr., D. S.; Balogh, D. T.; Dhanabalan, A.; Giacometti, J. A.; Zilio, S. C.; Oliveira Jr., O. N. *Polymer* **2001**, *42*, 6539-6544.

(30) Rochon, P.; Bissonnette, D.; Natansohn, A.; Xie, S. *Appl. Opt.* **1993**, *32*, 7211-7280.

(31) Song, O. K.; Wang, C. H.; Pauley, M. A. *Macromolecules* **1997**, *30*, 6913-6919.

(32) Takase, H.; Natansohn, A.; Rochon, P. *J. Polym. Sci.: Part B: Polym. Phys.* **2001**, *39*, 1686-1696.

(33) Sekkat, Z.; Yasumatsu, D.; Kawata, S. *J. Phys. Chem. B* **2002**, *106*, 12407-12417.

(34) Rodríguez, F. J.; Sánchez, C.; Villacampa, B.; Alcalá, R.; Cases, R.; Millaruelo, M.; Oriol, L. *Polymer* **2004**, *45*, 2341-2348.

(35) Fernández, R.; Mondragon, I.; Galante, M.; Oyanguren, P. *J. Polym. Sci.: Part B: Polym. Phys.* **2009**, *47*, 1004-1014.

(36) Gimeno, S.; Forcén, P.; Oriol, L.; Piñol, M.; Sánchez, C.; Rodríguez, F. J.; Alcalá, R.; Jankova, K.; Hvilsted, S. *Eur. Polym. J.* **2009**, *45*, 262-271.

(37) Sáiz, L. M.; Orofino, A. B.; Ruzzo, M. M.; Arenas, G. F.; Oyanguren, P. A.; Galante, M. J. *Polym. Int.* **2011**, *60*, 1053-1059.

(38) Dhanabalan, A.; Mendonça, C. R.; Balogh, D. T.; Misoguti, L.; Constantino, C. J. L.; Giacometti, J. A.; Zilio, S. C.; Oliveira Jr, O. N. *Macromolecules* **1999**, *32*, 5277-5284.

(39) Natansohn, A.; Rochon, P.; Gosselin, J.; Xie, S. *Macromolecules* **1992**, *25*, 2268-2273.

TABLE CAPTIONS

Table 1. Description of the samples used.

Table 2. Birefringence values and glass transition temperatures of the samples used.

Table 3. Remaining birefringence of thermosets containing 30 wt% $SBSep_{37}$ and different amounts of TAZ (10, 20 and 50 wt%).

Sample code	TAZ (wt%)	DGEBA/MCDEA (wt%)	SBSep (phr)
TAZ10	10	90	0
TAZ10-SBSep$_{37}$10	10	90	10
TAZ10-SBSep$_{37}$30	10	90	30
TAZ10-SBSep$_{37}$50	10	90	50
TAZ10-SBSep$_{46}$50	10	90	50
TAZ20	20	80	0
TAZ20-SBSep$_{37}$10	20	80	10
TAZ20-SBSep$_{37}$20	20	80	20
TAZ20-SBSep$_{37}$30	20	80	30
TAZ20-SBSep$_{46}$20	20	80	20
TAZ50	50	50	0
TAZ50-SBSep$_{37}$5	50	50	5
TAZ50-SBSep$_{37}$10	50	50	10
TAZ50-SBSep$_{37}$30	50	50	30
TAZ50-SBSep$_{46}$5	50	50	5

Table 1

Sample code	DO3 (wt%)	T_g (ºC)	Δn (10^{-2})	Δn_N (10^{-2})
TAZ10	2.58	155	0.33 ± 0.08	0.13
TAZ10-SBSep$_{37}$10	2.35	142	0.27 ± 0.03	0.11
TAZ10-SBSep$_{37}$30	1.98	121	0.24 ± 0.04	0.12
TAZ10-SBSep$_{37}$50	1.72	83	0.21 ± 0.01	0.12
TAZ10-SBSep$_{46}$50	1.72	79	0.20 ± 0.04	0.11
TAZ20	5.16	153	0.85 ± 0.14	0.16
TAZ20-SBSep$_{37}$10	4.69	141	0.81 ± 0.12	0.17
TAZ20-SBSep$_{37}$20	4.30	134	0.64 ± 0.09	0.15
TAZ20-SBSep$_{37}$30	3.97	122	0.55 ± 0.13	0.14
TAZ20-SBSep$_{46}$20	4.30	130	0.64 ± 0.01	0.15
TAZ50	12.9	139	1.90 ± 0.12	0.15
TAZ50-SBSep$_{37}$5	12.3	138	1.70 ± 0.08	0.14
TAZ50-SBSep$_{37}$10	11.7	134	1.70 ± 0.12	0.15
TAZ50-SBSep$_{37}$30	9.92	121	1.45 ± 0.32	0.15
TAZ50-SBSep$_{46}$5	12.3	138	1.80 ± 0.11	0.15

Table 2

Sample code	DO3 (wt%)	T_g (ºC)	rem^{60} (%)
TAZ10-SBSep$_{37}$30	1.98	121	41.4 ± 1.7
TAZ20-SBSep$_{37}$30	3.97	122	61.8 ± 0.4
TAZ50-SBSep$_{37}$30	9.92	121	69.7 ± 0.7

Table 3

FIGURE CAPTIONS

Figure 1. TM-AFM phase images of epoxy thermosets modified with 10 phr $SBSep_{37}$ containing: (a) 10 wt% TAZ, (b) 20 wt% TAZ and (c) 50 wt% TAZ; and epoxy thermosets modified with 30 phr $SBSep_{37}$ containing: (d) 10 wt% TAZ, (e) 20 wt% TAZ and (f) 50 wt% TAZ (3 μm x 3 μm).

Figure 2. TM-AFM phase images of epoxy thermosets containing 10 wt% TAZ and modified with 50 phr of: (a) $SBSep_{37}$ and (b) $SBSep_{46}$ (3 μm x 3 μm).

Figure 3. TM-AFM phase images of epoxy thermosets containing 20 wt% TAZ and modified with 20 phr of: (a) $SBSep_{37}$ and (b) $SBSep_{46}$ (3 μm x 3 μm).

Figure 4. TM-AFM phase images of epoxy thermosets containing 50 wt% TAZ and modified with 5 phr of: (a) $SBSep_{37}$ and (b) $SBSep_{46}$ (3 μm x 3 μm).

Figure 5. Typical writing, relaxing and erasing curves for systems containing 30 wt% of $SBSep_{37}$. The power of the writing beam is 6 mW.

Figure 6. Time necessary to achieve 80% of maximum birefringence as a function of: (a) $SBSep_{37}$ content and film thickness (in the inner graph is plotted the dependence on azobenzene ratio), and (b) power of the writing beam.

Figure 7. (a) Remaining birefringence after 60 s of turning *off* the writing beam as a function of $SBSep_{37}$ and TAZ content (in the inner graph is plotted the dependence on azobenzene ratio). (b) Residual fraction of birefringence after 45 h of turning *off* the writing beam for a film of TAZ50-$SBSep_{46}$5 (in the inner graph is plotted a magnification of the curve during first 4 min).

Figure 8. Successive writing-erasing sequences for a film of TAZ20-$SBSep_{37}$10: (a) from 1^{st} to 10^{th} cycle, (b) from 50^{th} -60^{th} cycle, (c) from 130^{th} to 140^{th} cycle and (d) from 260^{th} to 270^{th} cycle. The power of the writing beam is 6 mW.

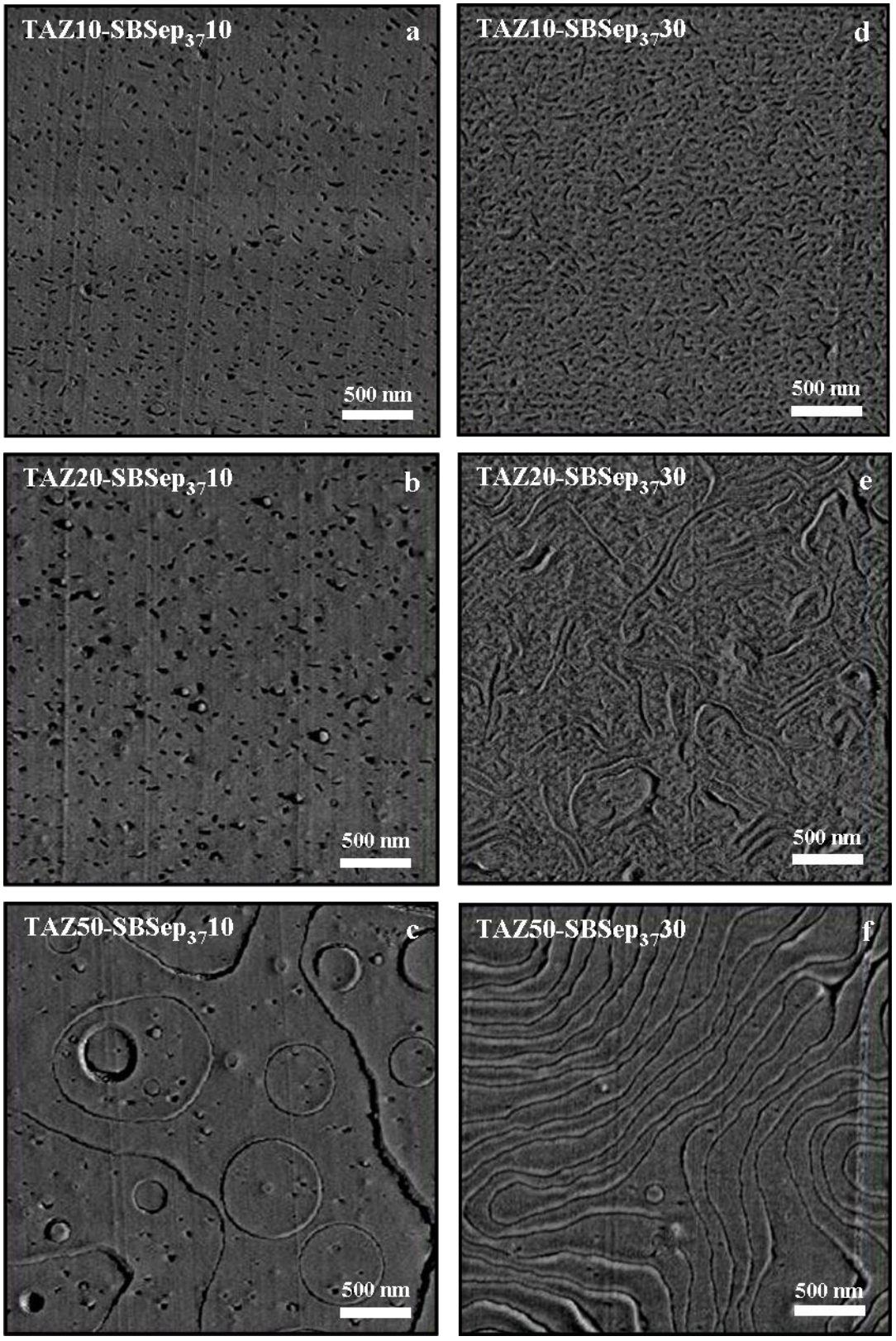
TAZ10-SBSep37 10
a
500 nm
TAZ10-SBSep37 30
d
500 nm
TAZ20-SBSep37 10
b
500 nm
TAZ20-SBSep37 30
e
500 nm
TAZ50-SBSep37 10
c
500 nm
TAZ50-SBSep37 30
f
500 nm

Figure 1

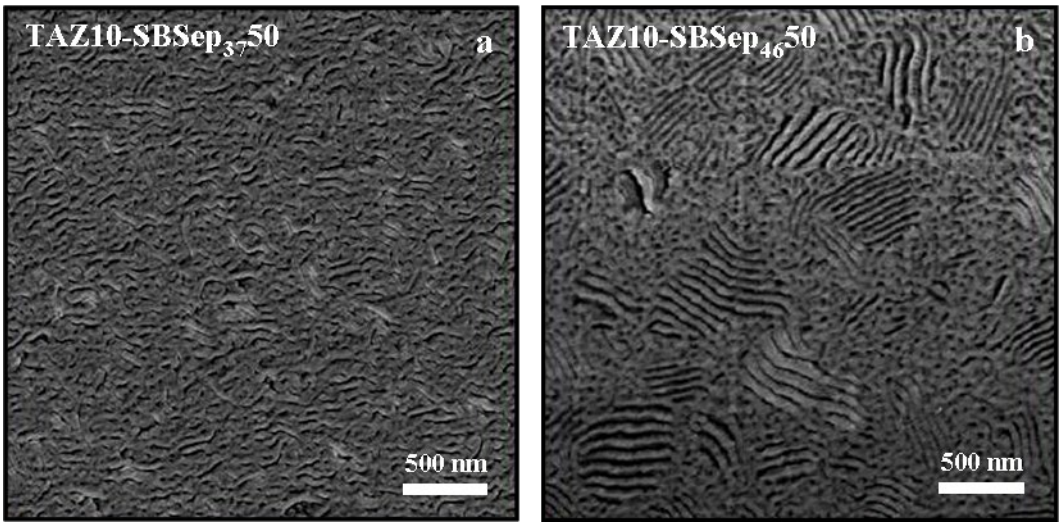

Figure 2

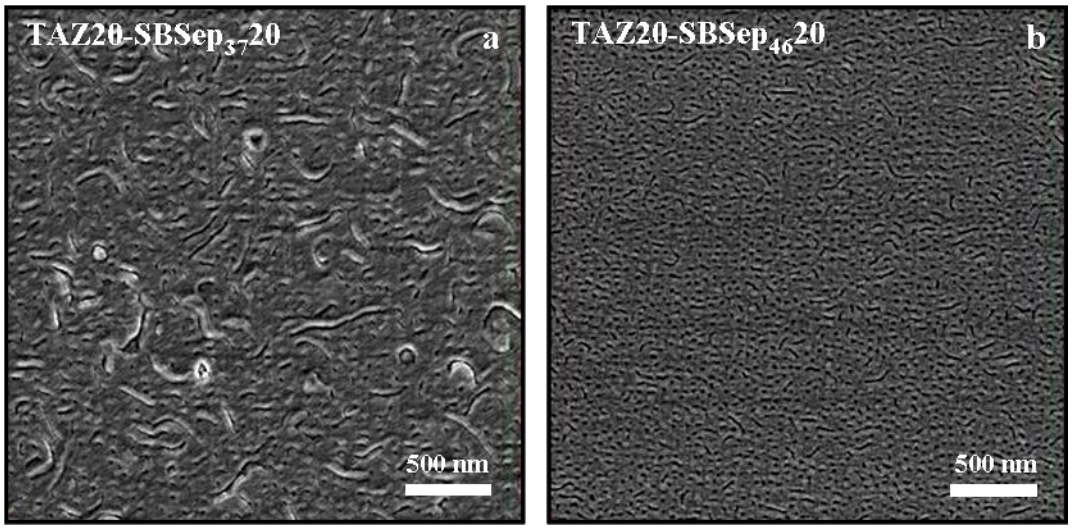

Figure 3

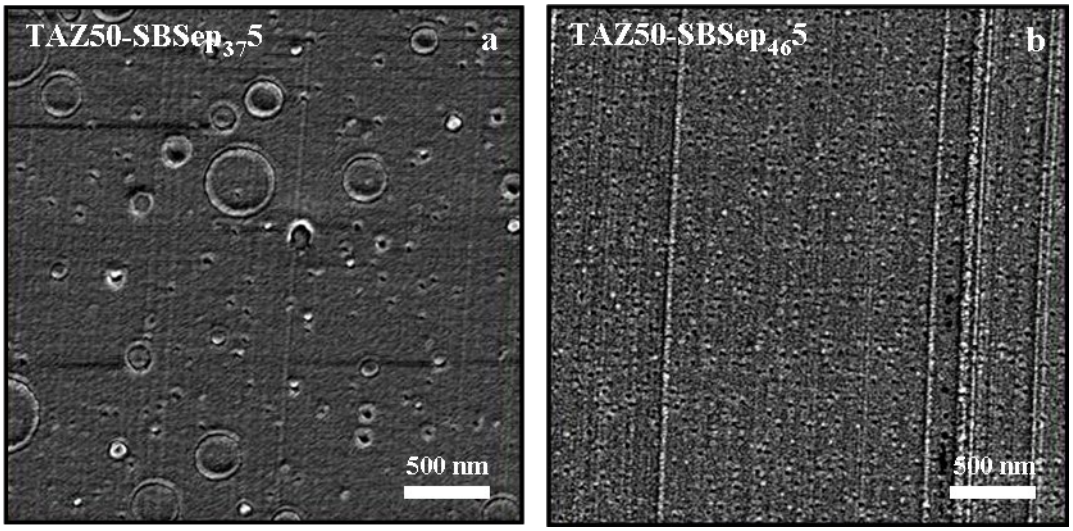

Figure 4

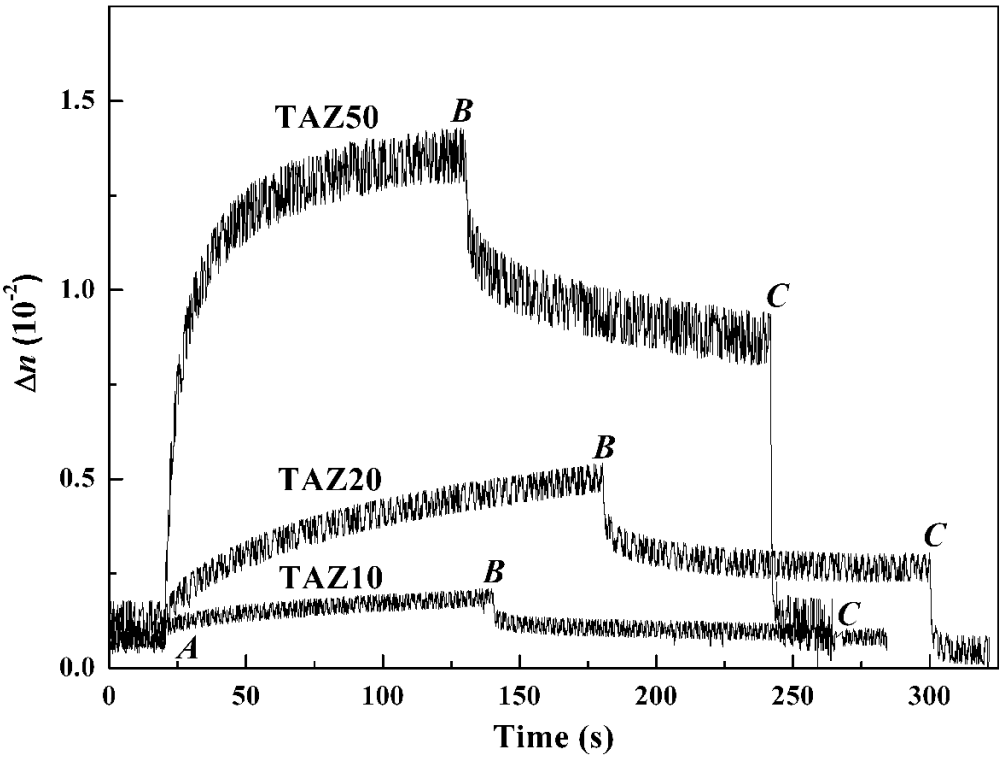
TAZ50
B
C
TAZ20
B
C
TAZ10
B
C
A
Δn (10-2)
Time (s)
0.0
0.5
1.0
1.5
0
50
100
150
200
250
300

Figure 5

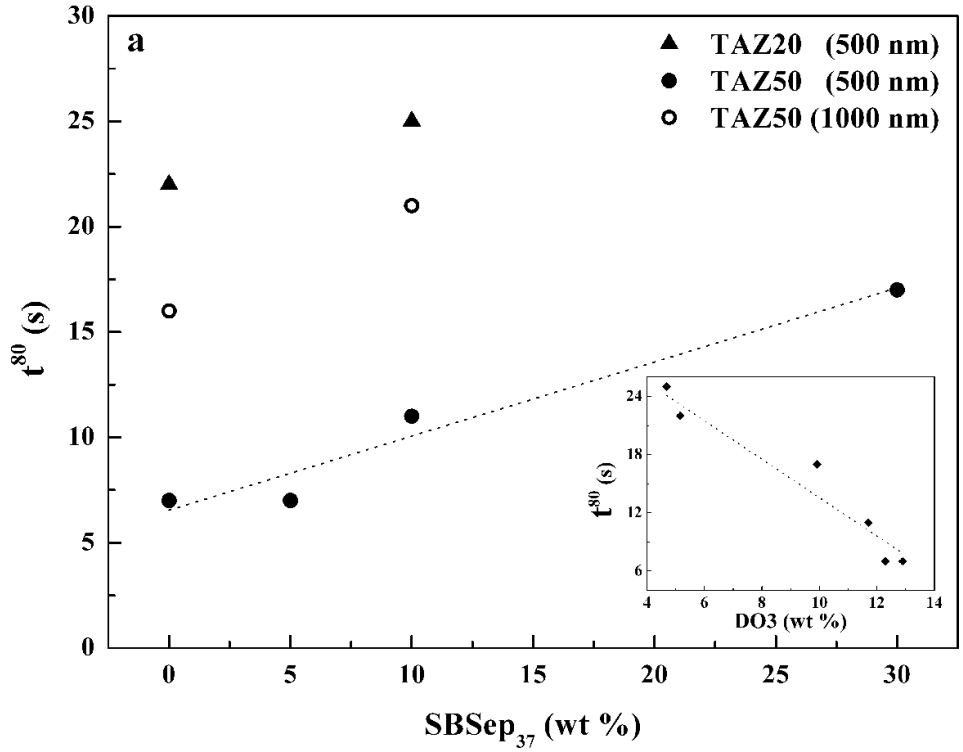
a
TAZ20 (500 nm)
TAZ50 (500 nm)
TAZ50 (1000 nm)
t^{80} (s)
SBSep$_{37}$ (wt %)
DO3 (wt %)

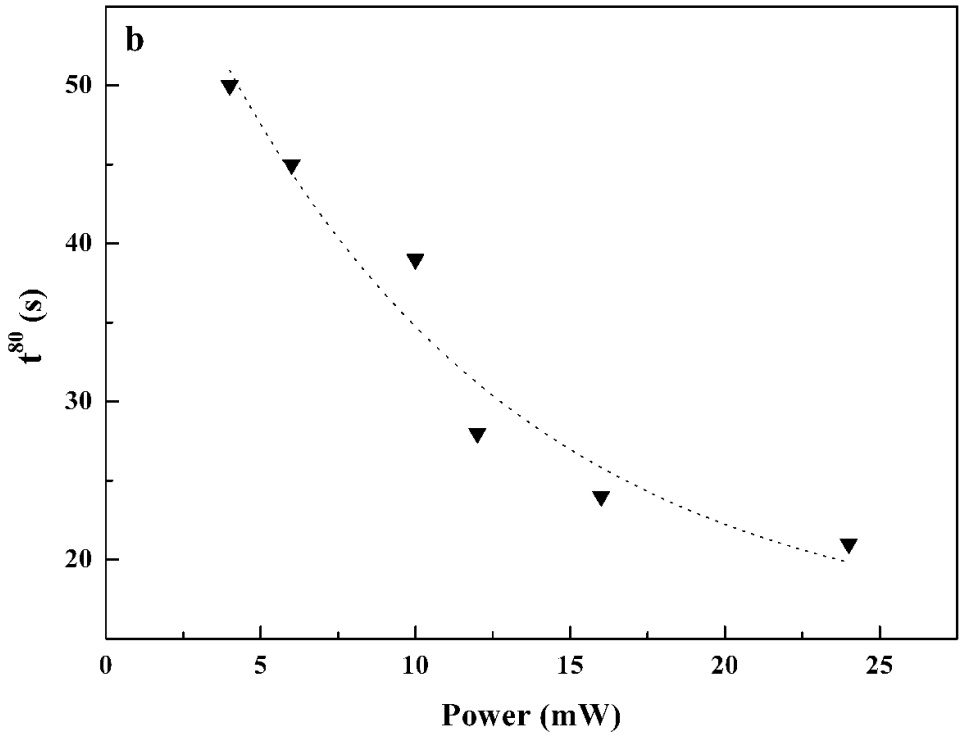
b
t^{80} (s)
Power (mW)

Figure 6

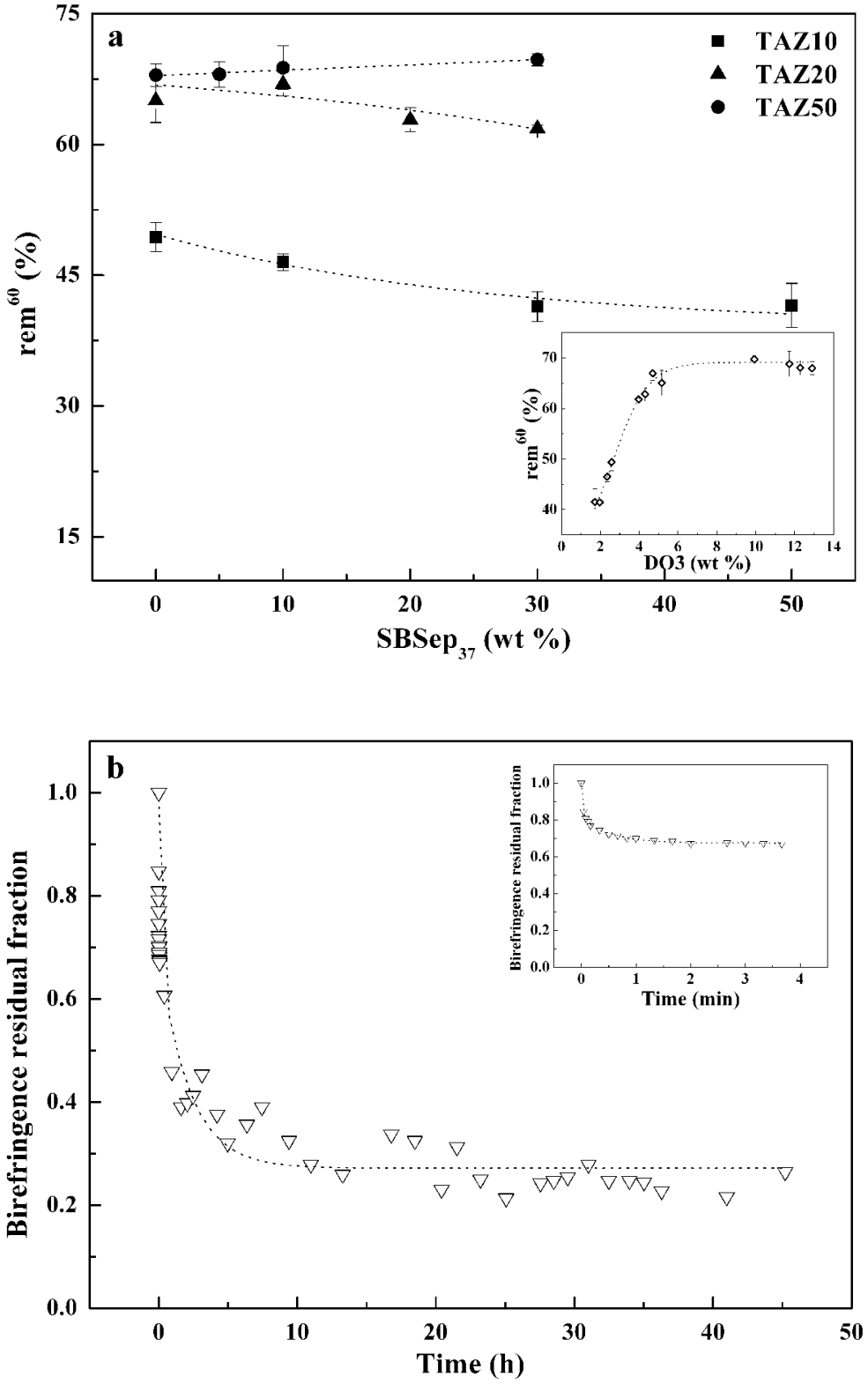
a
TAZ10
TAZ20
TAZ50
rem60 (%)
SBSep37 (wt %)
DO3 (wt %)
b
Birefringence residual fraction
Time (h)
Time (min)

Figure 7

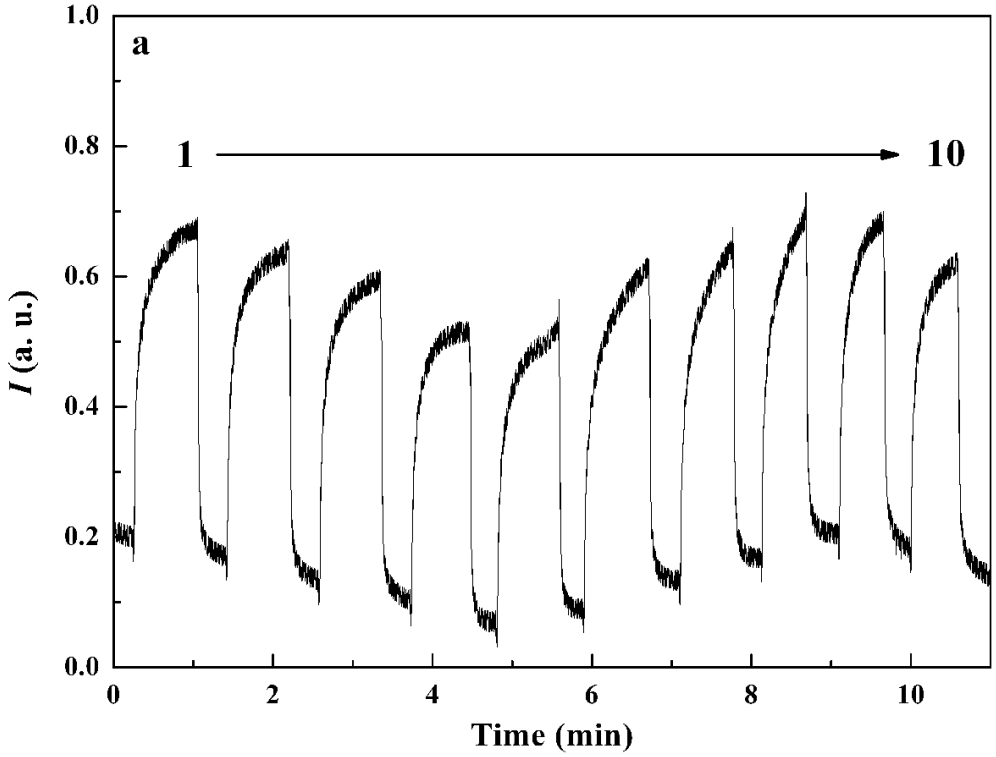
a
1
10
I (a. u.)
Time (min)
0.0
0.2
0.4
0.6
0.8
1.0
0
2
4
6
8
10

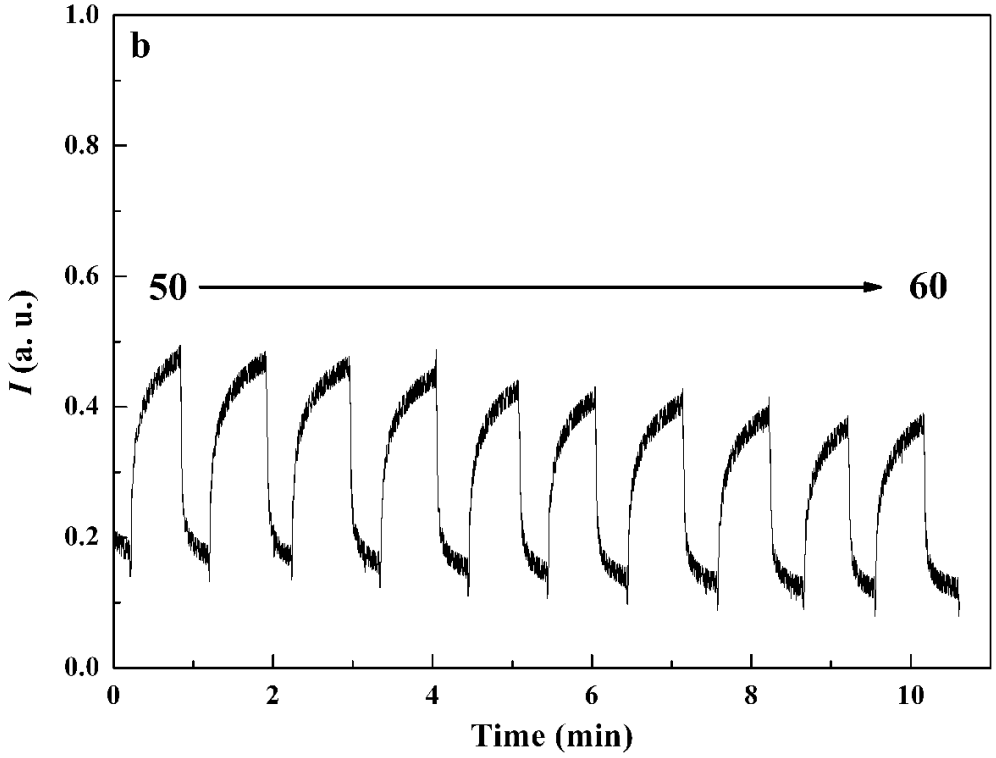
b
50
60
I (a. u.)
Time (min)
0.0
0.2
0.4
0.6
0.8
1.0
0
2
4
6
8
10

Figure 8

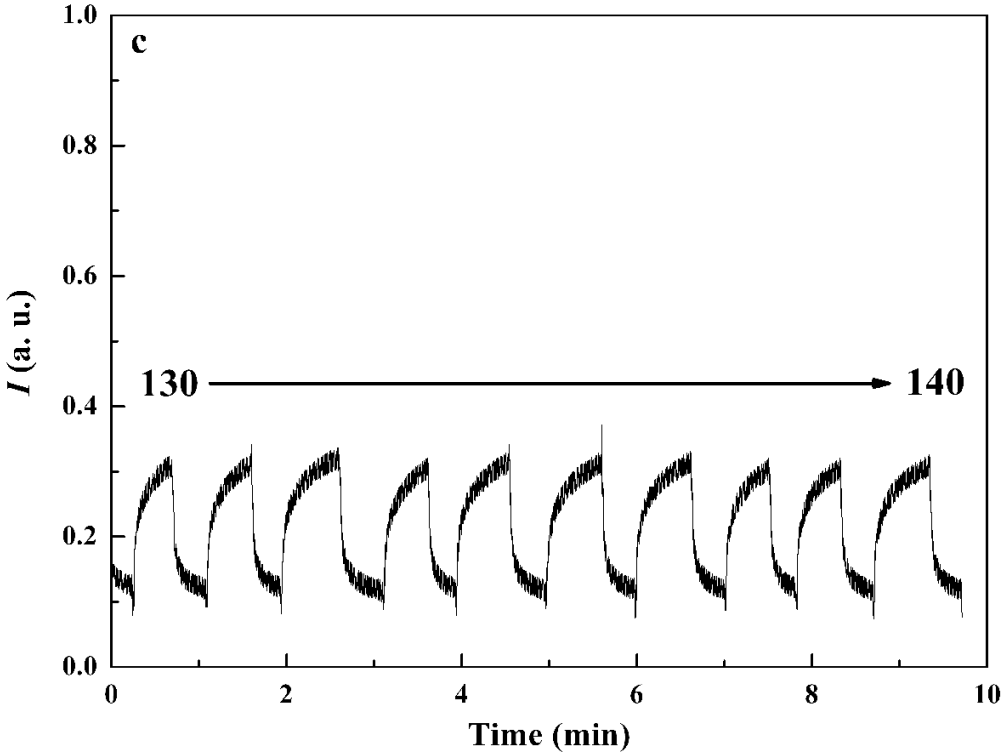
c
130
140
I (a. u.)
Time (min)
0.0
0.2
0.4
0.6
0.8
1.0
0
2
4
6
8
10

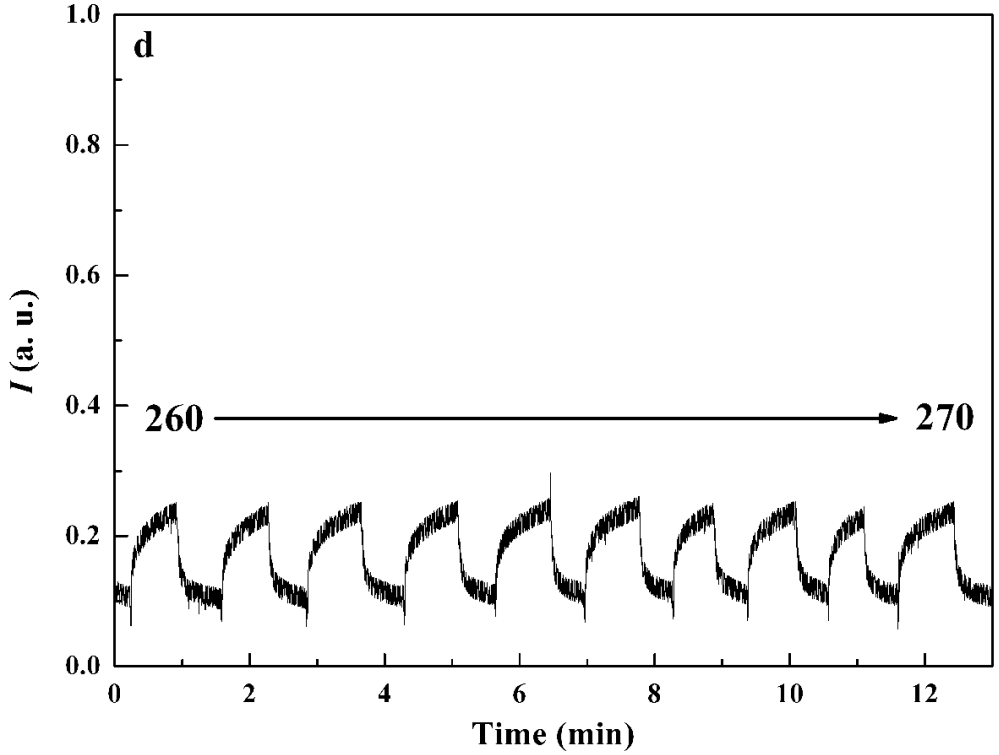
d
260
270
I (a. u.)
Time (min)
0.0
0.2
0.4
0.6
0.8
1.0
0
2
4
6
8
10
12

Figure 8